A Mechanical Hand-Tracking System with Tactile Feedback Designed for Telemanipulation

Marcello Palagi[1,2], Giancarlo Santamato[1,2], Domenico Chiaradia[1,2], Massimiliano Gabardi[1,2], Simone Marcheschi[1,2], Massimiliano Solazzi[1,2], Antonio Frisoli[1,2], Daniele Leonardis[1,2]

***Abstract*—In this paper, we present a mechanical hand-tracking system with tactile feedback designed for fine manipulation in teleoperation scenarios. Alternative tracking methods based on artificial vision and data gloves have become an asset for virtual reality interaction. Yet, occlusions, lack of precision, and the absence of effective haptic feedback beyond vibrotactile still appear as a limit for teleoperation applications. In this work, we propose a methodology to design a linkage mechanism for hand pose tracking purposes, preserving complete finger mobility. Presentation of the method is followed by design and implementation of a working prototype, and by evaluation of the tracking accuracy using optical markers. Moreover, a teleoperation experiment involving a dexterous robotic arm and hand was proposed to ten participants. It investigated the effectiveness and repeatability of the hand tracking with combined haptic feedback during a proposed pick and place manipulation tasks.**

***Index Terms*—teleoperation, hand-tracking, exoskeleton, Screw Theory, haptic feedback.**

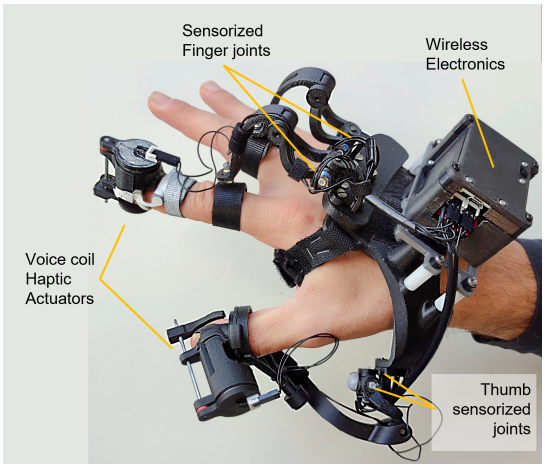

Fig. 1. The proposed mechanical hand-tracking system endorsing serial kinematic chains for precise fingers pose estimation and voice-coils on the fingertips for tactile feedback.

I. Introduction

THE quality of manipulation becomes essential when telemanipulation tasks are performed in critical scenarios [1], [2], [3]. In such a context, precise hand-tracking and high quality haptic information are crucial factors in terms of the stability of the grasp, inside-hand, and fine manipulation.

Nowadays optical tracking technology represents an asset in a variety of applications due to the immediateness of use and together with the widespread of virtual reality systems. Yet optical fingers tracking has to deal with silhouette scales, the unavoidable occlusions which are due to the interposition of obstacles between the cameras and the designated surfaces, but also to fingers overlapping that might occur in certain manipulation pose [4], [5]. Besides purely optical devices exclude the sense of touch.

On another side, data gloves are a commonly used solution in virtual reality interactions and video-gaming. These systems offer the facility of integrating a large variety of sensors with adequate transparency and wearability. Resistive bending sensors [6] are commonly used to measure the flexion of the fingers, while inertial measurement units (IMU) can be embedded to capture also the hand orientation [7], [8]. Nonetheless, a lack of precision may occur due to unavoidable slips which happen between the bending sensors and the fingers and also between the IMU and the hand. As a consequence, gloves seem less suitable than optical-based devices for remote manipulation tasks [8]. On the other hand, optical tracking suffers from occlusion, especially for hand tracking where fingers are in close proximity one each other. Robust setups require multiple camera systems and free line-of-sight with the tracked hands, as in the setup used in [8]. Besides, introducing actuators at the fingertips of data gloves can be a concern when IMU with magnetometers are employed, due to electromagnetic interference. A more recent technique implemented in commercial tracking systems (i.e. Ultraleap or Oculus Quest 2 hand tracking systems) is based on cameras and artificial vision. Robustness is not guaranteed in case of occlusions and bimanual interaction, moreover, the addition of haptic actuators, changing the shape of the hand, can affect the quality of the tracking.

So far two different approaches to haptic feedback have been mainly investigated: on one side, kinaesthetic force feedback provided by active hand exoskeleton devices [9], and on the other side, tactile feedback rendered by fingertip devices [10]. While the latter does not apply an absolute force opposing finger closure but renders only cutaneous perception at the fingerpad, they have the advantage of significantly smaller design and enhanced wearability. Data gloves have been proposed using inexpensive and easy to implement vibrotactile actuators [11]. Beyond vibrotactile cues, more

[1] are with the Institute of Mechanical Intelligence, Sant'Anna School of Advanced Studies, Pisa, Italy name.surname@santannapisa.it

[2] are with the Department of Excellence in Robotics & AI, Scuola Superiore Sant'Anna

The publication was created with the co-financing of the European Union - FSE-REACT-EU, PON Research and Innovation 2014-2020 DM1062 / 2021

informative haptic stimuli can be rendered especially in fine manipulation tasks, where both dynamic transients and fine modulation of the grasping force play a significant role [12], [13]. Several tactile devices at the state-of-the-art have been applied in virtual reality [14] and telemanipulation [15], [16]).

In this paper, we introduce a Mechanical Hand-Tracking (MHT) system, Fig. 1, combining accurate finger tracking and high mobility with tactile stimulation. In particular, the use of a serial kinematic chain mechanism for fingers tracking is investigated under lightweight and full fingers mobility requirements. The device includes voice-coils actuators for rendering tactile feedback at fingerpads. With respect to optical tracking systems, the proposed device guarantees continuous finger tracking for all the hand poses, since it is exempt from occlusions and, besides it provides a higher communication rate which is crucial for the stability of teleoperation. At the same time, it allows the chance of integrating actuators for fingertip stimulation which often represents a challenge for data gloves due to electromagnetic interference. Underactuated hand exoskeleton can be considered closely related devices, with kinematics adapting to the finger, as i.e. in [17], [18] and tracking capabilities. However, there the kinematic chain is conceived and optimized for exerting forces rather than for tracking purposes (i.e. in [9], to apply linear forces without torques to the finger segments) with limits in workspace and transparency.

In this work, we present the theoretical design of the Parallel Kinematic Chains (PKC) that constitute the tracking device: in particular, an intuitive graphical methodology - based on the screw theory - is proposed to define the number, position, and orientation of the PKC joints. Such a procedure is proven to satisfy the complete finger mobility requirement with the minimum number of PKC joints.

Then, we present development of a prototype and experimental validation of the tracking accuracy using optical markers. Moreover, the suitability of the device for telemanipulation purposes was validated during a teleoperation pick and place task with haptic feedback, involved untrained participants.

II. Design of the Mechanical Hand-Tracking System

A. Kinematic Hand Model

In this work, the classical kinematic hand model proposed in [19] and [20] is adopted. For the sake of clarity, Fig. 2 (a) and (b) report the nomenclature for the long fingers and the thumb, respectively.

In particular, it is assumed that:

- the Flexion-Extension (F-E) axes are parallel;
- the F-E rotations are decoupled from the Adduction-Abduction (A-A) rotations;
- the F-E axis and the A-A axis are incidents;
- the position and orientation of all the joints axes is constant in the entire range of motion;

Consequently, the long finger kinematics can be represented by a Serial Kinematic Chain (SKC) with 4 DoFs, as shown in Fig. 2a, while a 5-DoFs scheme is adopted for the thumb, Fig. 2b. Such a hand model is necessary to design the MHT device (see Sec. II-B). A preliminary choice concerns the location of the anchor point between the finger and the MHT chain. Note that this point coincides with the end-effector of the chain introduced by the MHT. In this regard, several aspects have been considered, such as: i) ergonomics; ii) size; iii) finger mobility; iv) the encumbrance of the haptic interface on the distal phalanx. Consequently, the anchor point is located on the proximal phalanx for the long fingers, while it occurs on the distal phalanx for the thumb.

B. Screw Theory Approach to the Kinematic Design

The main objective of the kinematic design is to find the strictly necessary number of PKC joints/DoFs that ensures full finger mobility. Indeed, the introduction of additional DoFs might result in: i) increased complexity and weight; ii) further control effort in the case of telemanipulation; iii) redundancy, i.e. non-uniqueness of a single MHT configuration for a given configuration of the finger. In the following, all the axes of the PKC are represented via pin joints due to size constraints, the simplicity of construction, [21], and easiness in potentiometer sensors installation.

To this purpose, the Screw Theory (ST) methodology is adopted ([22], [23]). A screw vector is an $\mathbb{R}^{6x1}$ element that can be expressed as a Twist $\underline{\xi}$ or a Wrench $\underline{\zeta}$ term ([22]). The Wrench can be represented as a pure force or a pure moment while the Twist can be represented as a pure rotation or a pure translation. With the purpose of fingers mobility, the choice of MHT joints position and orientation is subjected to the so-called *Reciprocity Condition* (RC), expressed by the following Eq. 1:

$$\underline{\xi} \circ \underline{\zeta} = \underline{\zeta} \circ \underline{\xi} = (\Pi(\begin{pmatrix} \underline{\zeta_F} \\ \underline{\zeta_M} \end{pmatrix}^T \begin{pmatrix} \underline{\xi_R} \\ \underline{\xi_T} \end{pmatrix}) = \underline{\zeta_F}^T \underline{\xi_T} + \underline{\zeta_M}^T \underline{\xi_R} = 0 \tag{1}$$

where $\Pi = \begin{pmatrix} 0_{3x3} & I_{3x3} \\ I_{3x3} & 0_{3x3} \end{pmatrix}$: is called the permutation matrix; $\underline{\zeta_F}$, $\underline{\zeta_M}$, $\underline{\xi_R}$, and $\underline{\xi_T}$ are force components, moment components, rotational velocity components and linear velocity components, respectively.

The wrenches that satisfy the RC are called *structural*. Since n-DoFs may be always deemed as n independent twists, the structural wrenches can be interpreted as the forces/moments that do not cause a speed variation on any of the DoFs, i.e. they do not develop mechanical power. In other words, the RC allows to find the wrenches of a SKC that oppose to the mobility of its joints.

More intuitively, the RC can be expressed through the following graphical conditions:

1) a force and a rotation are reciprocal if their directions are parallel or they intersect a a point;
2) a moment and a rotation are reciprocal if their directions lie in two orthogonal planes;
3) a force and a translation are reciprocal if their directions lie in two orthogonal planes;
4) a moment and a translation are always reciprocal.

For a better understanding of the RC, Fig.3b reports an example showing all the wrenches and twists in the case of a single pin joint, Fig.3a, and a two pin joint, Fig.3b. In

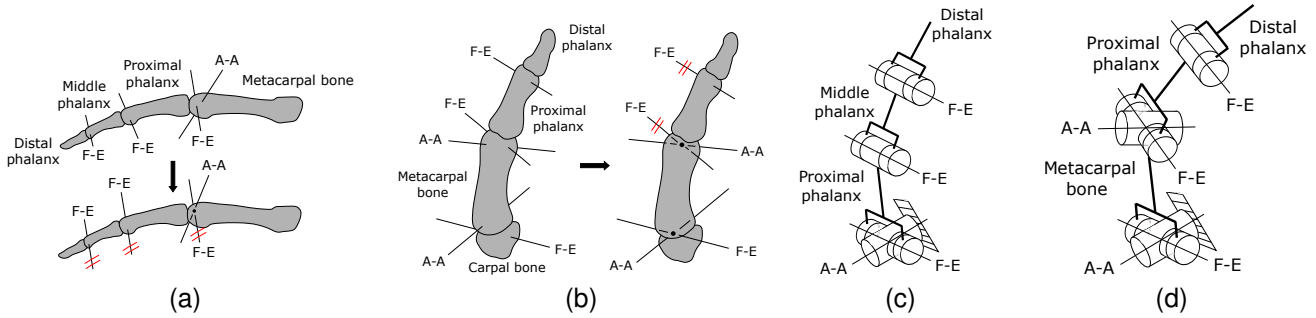

Fig. 2. Kinematic hand model for the long fingers (a), and the thumb (b). Simplified Serial Kinematic Chains for the long fingers (c) and the thumb (d)

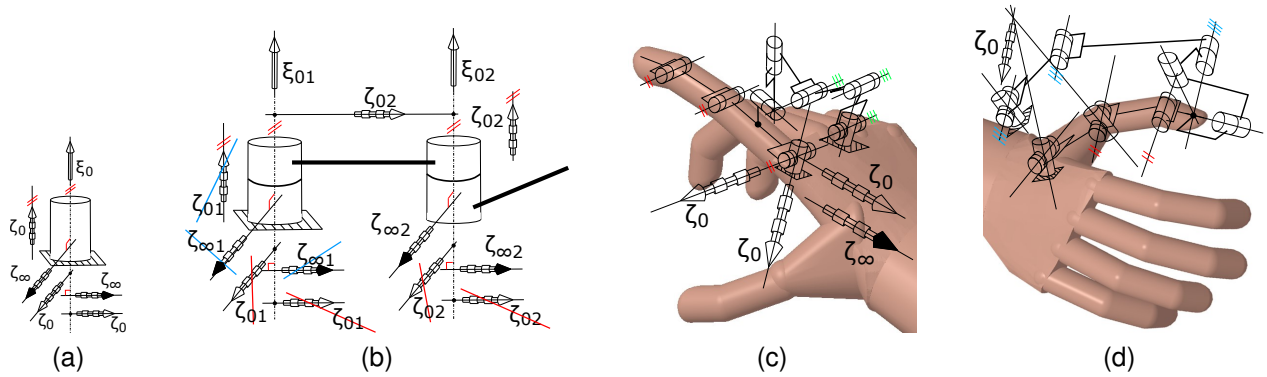

Fig. 3. Wrenches (black: moment; white: force) and Twists for a single pin joint, (a), and a two pin joints (b). The two pin joints configuration has 4 structural wrenches (2 forces and 2 moments). Parallel kinematic chains and structural wrenches for the long fingers, (c), and the thumb, (d).

the figure, the subscript 0 stands for the force component of the wrench, while ∞ stands for the moment component. In Fig.3a all the depicted wrenches are structural because they are orthogonal against the axis of the pin and, consequently, no rotational velocity is produced. Instead, in Fig.3b, both the force wrenches ζ_{01} are ineffective on the twist ξ_{01}, still they are not structural (red deletion) because their directions are orthogonal against the axis of joint 2. A similar consideration applies to the wrenches ζ_{02}. On the contrary, the moment wrenches $\zeta_{\infty 2}$ are structural because they are orthogonal against both the twists ξ_{01} and ξ_{02}. It should be also considered that some wrenches are redundant (blue deletion), such as the moment wrench $\zeta_{\infty 1}$ because it is parallel to the wrench $\zeta_{\infty 2}$.

Finally, we aim to find the residual wrenches that must be eliminated to guarantee mobility of the chain ζ_{SKC_i}. These can be determined by retaining only the unique structural wrenches of the chain [22]:

$$\zeta_{SKC} = \bigcap_{j=1}^{f} \zeta_j \tag{2}$$

Let us now consider a parallel kinematic chain with m SKCs and a single end-effector in common. Then the structural wrenches of the PKC at this end-effector (ζ_{PKC}) are obtained as a linear combination of all the residual wrenches that are included in each chain before the end-effector:

$$\zeta_{PKC} = \sum_{i=1}^{m} \zeta_{SKC_i} \tag{3}$$

It turns out that the MHT does not introduce structural wrenches in the finger SKC if 6 joints with 6 DoFs (6 independent Twists) are introduced. Consequently, the introduction of additional DoFs is detrimental because it would imply redundancies in the MHT. The adopted designs are shown in Fig.3c and in Fig.3d for the long fingers and the thumb, respectively. In both cases, the MHT chain has 6 DoFs and it leaves the structural wrench of the fingers unchanged. In Fig.3c, the structural wrenches are located on the proximal phalanx, while they fall on the distal phalanx, Fig.3d, for the thumb. Some details about Fig.3:

- the pattern drawn under the universal joints stands for the grounded body. In the case of the fingers SKC, it coincides with the metacarpal bone;
- the last 3 pin joints in the MHT for both the long fingers and the thumb collide in a single spherical joint, intersecting their axes together. In the same fashion, also the first 2 joints collide in a single universal joint. This choice further reduces the size of the device;
- the natural wrench in the PKC thumb is a force vector along the line created by the intersection of the planes containing the universal joints of the thumb SKC.

C. Optimization of the link lengths for the elimination of kinematic singularities and adaptability to finger dimensions

Notwithstanding the achievement of full fingers mobility, operations of a MHT can still be limited due to singularities that might occur in certain hand poses. In this regard, a

numerical routine is proposed to adjust the lengths of the MHT kinematic chains. For both the PKCs of the long fingers and the thumb, singularities occur when the joint between Link 1 and Link 2 (Fig.4) falls on the line joining the centers of the universal joint and the ball joint. In such a configuration, the mechanism results locked and finger tracking is not possible. Since complete locks elimination is not feasible, a possible solution is to make singularities fall outside the workspace of the fingers. For the sake of simplicity, the kinematics of the PKCs is assumed planar Fig. 4, as in [22], since the universal joint and the ball joint follow the orientation of the fingers. Thus the PKC kinematics can be represented by a simple four bar scheme, where Link 1 and Link2 represent the MHT, and Link 3 is the pose vector of the phalanx. Because redundancies have been excluded, as described in Sec. II-B, then there exists a single condition that avoids the singularities in the fingers workspace. This condition is expressed by: $0 < \varepsilon < \pi$ where ϵ is the angle between the Link 1 and the Link 2 in Fig. 4. According to the well-known kinematics of a four linkage bar mechanism, this angle is a function of the MHT links lengths L_1 and L_2.

On another side, a further requirement is to ensure the adaptability to different fingers size. Such a dimension can be considered proportional to the length of the Link 3. At this point, a numerical routine has been contrived to find the values of the MHT links that simultaneously satisfy the no-singularities and the size-adaptability requirements. First, the kinematics of the four bar mechanism was solved analytically using the well-known closing equations in which all the angles have been referred to the absolute orientation of the Link 3. This choice is motivated by the fact that this angle defines the position of the end-effector against the metacarpal-phalangeal joint for the long fingers. From the acquisition of this value, it is possible to estimate the values of each angle, including the angle ϵ, and the orientation of the proximal phalanx for the long fingers, and the orientation of the distal phalanx for the thumb. Besides in the closing equations, the length of the Link 2 is expressed by the non-dimensional parameter k which normalizes the link length against L_1.

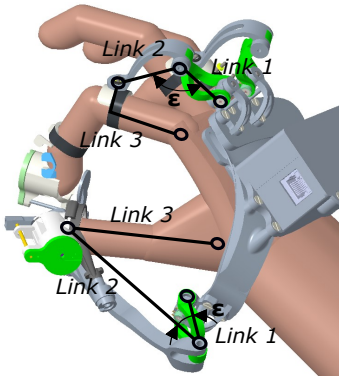

Fig. 4. Singularity angle ε for the long fingers PKC and the thumb PKC

Hence the kinematics of the MHT can be parameterized for any given hand size, represented by L_3. At this point, all the MHT configurations have been explored by letting L_3 to vary within the mean and standard deviation interval proposed by [24], while k varies in the interval $[0.5 - 3]$ which has been defined for encumbrance and design limits. Only the configurations showing admissible values of ϵ were retained. Finally, for a given L_1, the lowest value of k is chosen among the admissible set with the aim to optimize the encumbrance. As an example, a first prototype of the MHT has been designed with the following parameters: i) thumb: L_1=24.4 mm, k=3.45 (L_2=84.2 mm); index finger: L_1=24 mm, k=2.15 (L_2=51.6 mm); middle finger: L_1=26 mm, k=2.09 (L_2=54.3 mm).

D. Hand Tracker Prototype Implementation

A prototype of the MHT device, shown in Figure 1, has been implemented for experimental validation. The links of the MHT have been printed in nylon (Onyx filament printed with Markforged Mark Two printer). The device is composed of three serial kinematic chains, one for the thumb, one for the index, and one for the middle. Each serial kinematic chain has been designed to allow complete mobility of the corresponding finger. Different fingers size has been considered, by optimizing the lengths of the serial kinematic links to ensure adaptability for a number of finger dimensions. The workspace of each serial kinematic chain coincides with the workspace of the user's finger. Besides, each kinematic chain is located on the side of the backhand. Consequently, also the interaction between the fingers – like in complete closure poses – implies a minimum interference which is due only to the encumbrance of the haptic fingertips. A wide-bandwidth haptic actuator, based on an electromagnetic voice coil, is mounted on the index and the thumb (for actuators characterization see [25]). Miniature potentiometers (outer diameter 8mm, thickness 2mm) have been used to sensorize two joints for the thumb, and one joint for the index and middle finger, according to the envisaged teleoperation with the MIA robotic hand. With respect to other angular position sensors (i.e. optical or magnetic encoders), the miniature potentiometers resulted more compact. Introduced friction in the mechanism was very low: peak friction force at the fingertip was measured below 30 mN, using an Optoforce 10N force sensor, in contact with the finger link and passively moving the mechanism and the potentiometer.

The control and communication interface of the device was implemented with an embedded electronic board based on the Espressif ESP32 micro-controller, providing also Wi-FI communication with the host PC. The board was battery-powered at 3.7V by a Li-Po Cell. Two DRV8835 Texas Instruments H-Bridges IC were integrated into the board to drive the two haptic actuators. An Inertial Measurement Unit (Bosch BNO055) has been embedded at the hand dorsum to provide the orientation of the hand. The weight of the entire system, including electronics and voice coils, is 228 g and it is subdivided into its components: 27 g for the thumb voice coil; 24 g for the index voice coil; 20 g for the thumb SKC; 11 g for both index SKC and medium SKC; 47 g for the device frame; 59 g for the electronics box; 29 g for the battery.

III. Experimental Tests and Validation

We designed two tests to validate the mechanical design and the haptic features of the implemented prototype: i)

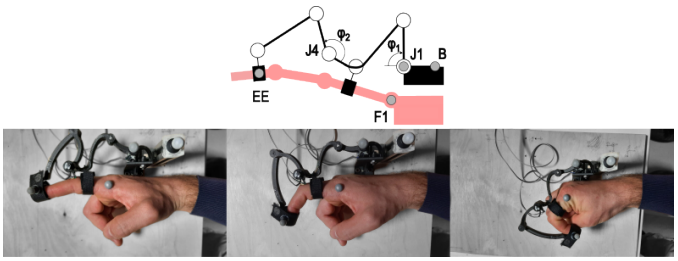

Fig. 5. Experimental tests for the characterization of the tracking accuracy.

TABLE I
ESTIMATED ERROR ON THE FINGERTIP POSITION FOR DIFFERENT INDEX POSES

Config.	$\varphi_1(^\circ)$	$\varphi_2(^\circ)$	Error (mm)	Error rel (%)
1	101.6	-136	3.65	3.07
2	143.7	-140	5.61	4.1
3	147.3	-103	2.45	1.77
4	155.6	-145	0.95	0.67
5	161	-163	3	2.17
6	168	-174.5	2.73	2

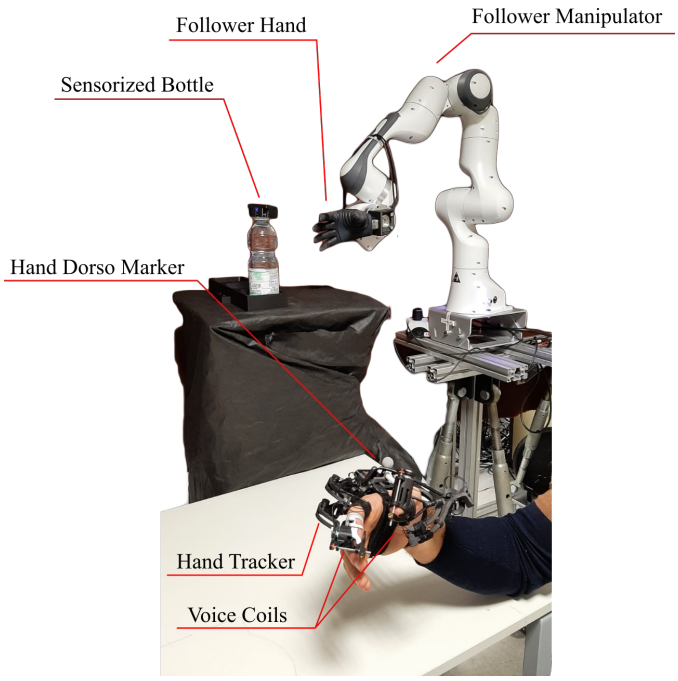

Fig. 6. Experimental tests for the evaluation of the manipulation performance during a teleoperation scenario.

characterization of the tracking accuracy; ii) a teleoperation pick-and-place task with haptic feedback.

A. Characterization of the Tracking Accuracy

A first characterization was performed with the aim to evaluate the measurement accuracy of the MHT. To this end, the hand-tracking measurement is compared with a ground-truth reference, represented by the measurement of an optical tracking system (Optitrack V120 Trio). Motion Capture was adopted as the optical system, consisting of a set of cameras that record the position of markers placed on the user's hand. An example of the layout is pictured in Fig. 5, for the case of the long fingers. One marker E_E was placed on the fingertip, which represents the end-effector, and a second marker, F_1 was placed on the joint between the metacarpal bone and the proximal phalanx, to provide the position of the hand dorsum with respect to the tracker. Two auxiliary markers B and J_1 were introduced to mimic the tracker reference frame and define the coordinate axis for the kinematic equations.

On the other side, the tracker is endorsed with two potentiometers devoted to estimating the angles φ_1 and φ_2 of the joint J_1 and J_4, respectively. From these measurements, the tracker estimated the position of the fingertip by solving the kinematics of the parallel chain constituted by the tracker and the finger. Finally, the two positions of the end-effector, one estimated by marker (reference) and one reconstructed by the tracker, could be compared to calculate the error of the tracker accuracy. The error estimate was derived for six poses of the finger, including complete flexion, complete extension, and four intermediate configurations. The frequency of acquisition was 150 Hz and the distance of 1.5 m between the cameras and the target. Results are listed in Tab. I in the form of absolute error, expressed in mm, and relative error (normalized against the estimation of the optic system). The error in the complete extension configuration is 3.65 mm, while it is reduced to 2.73 mm in the complete closure pose. The minimum and maximum error values are found for two intermediate configurations (0.95 mm and 5.61 mm). These results are adequate for the intended use in teleoperation scenarios.

B. Comparative Telemanipulation Tests

The goal of our experimental study is to evaluate the effectiveness of the MHT device to perform hand-tracking with simultaneous tactile feedback for telemanipulation purposes.

To this end, a teleoperation scenario was set up, as shown in Fig. 5 (right). On one side, the operator is wearing the MHT device for hand pose tracking. In the setup, an optical marker was used for tracking of the hand position. Namely, a 7 DoFs Franka Emika Panda arm was mounted with a vertical layout, with the purpose of mimicking the human arm configuration. The Prensilia MIA Hand, chosen as teleoperated hand device, allows replication of 80% of human daily-gestures, like cylindrical grip, precision grip, and lateral grip. It endorses independent F-E for the thumb, the index, and the middle, and A-A for the thumb. Consequently, the MHT was equipped with four potentiometer sensors to track the same hand kinematics DoFs. An illustration of the telemanipulation architecture is depicted in Fig. 7 in which the leader's and follower's system components and the exchanged signals are summarized.

The hand tracker prototype, the optical tracker, and the teleoperated robot communicated through UDP/IP protocol using mixed wireless and wired connections. A host PC running a

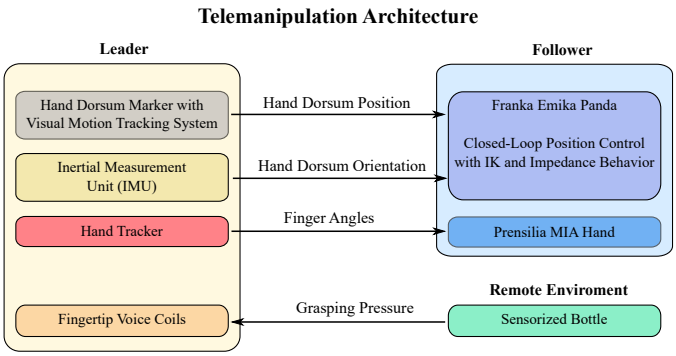

Fig. 7. Control architecture of the telemanipulation system. The master system imposes the hand dorsum pose and the fingers flexion/extension angle. The remote environment was sensorized with a pressure sensor and feed-back the grasping relative pressure on the bottle. The master operator perceives the remote environment through a force interaction with the fingertip haptic device - voice coils.

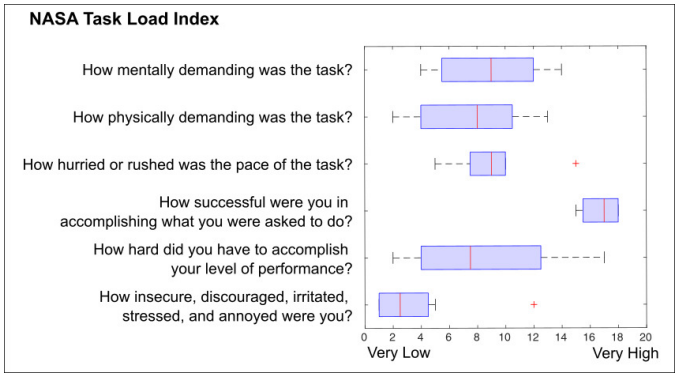

Fig. 8. Results of the NASA questionnaire proposed to participants

Matlab Simulink model in real-time merged information from the leader and follower sides.

The proposed task is the pick-and-place of a sensorized water bottle. Namely, it is required to extract the bottle from a plastic slot and place it in a nearby slot. The task is considered failed if the bottle falls after the first grasping or during the pick and place execution. The distance between the master operator and the robotic arm was about 1 m. Because no precise force feedback was provided by the robotic hand, a pressure sensor (Bosch BMP280) was mounted under the cap and used to modulate tactile feedback at the MHT. Ten healthy subjects were involved in the experiment: 6 males and 4 females; age interval: 24-33 years old. All of the participants had experience in robotic systems, although eight of them had no previous experience in teleoperation. The experimental procedures were approved by the Ethical Review Board of Scuola Superiore Sant'Anna (approval number 152021).

The task was proposed to participants with two different target objectives:

- TEST A: fast manipulation - the user was asked to succeed in the task as fast as possible in a row of 10 trials;
- TEST B: precise manipulation - the user was asked to succeed in the task with the highest rate of success in a row of 5 trials, with no timing constraint, and with the explicit indication to perform a grasp "as soft as possible" without compromising the completion of the task.

Both experimental conditions were performed with (w HF) and without (w/o HF) haptic feedback. The sequence of the four possible experimental conditions was randomized. The quantitative assessment of the task was evaluated through: i) the average time to complete a trial; ii) the success rate; iii) the average grip pressure and iv) the average standard deviation of the grip pressure as an index of the variability of the leader operator's grasping pressure.

For each participant, performance indexes were averaged among all the trials in the same experiment and statistical tests were performed to detect potential significant differences among conditions. We checked the normality of the analyzed dataset and performed a Kruskal-Wallis non-parametric test (for not normally distributed set) or the one-way ANOVA test (for a normally distributed set) on the following comparisons: average grip pressure between w HF and w/o HF, and grasping pressure variability in task w HF or w/o HF.

Finally, a NASA Task Load Index questionnaire was proposed to subjects at the end of the experiment.

IV. Results and Discussion

Validation of the fingertip tracking accuracy for the long finger mechanism reported a mean error of 3 mm: this shows a noticeably better performance than data gloves and vision-based systems compared in [8]. Optical tracking with markers, used in [8] and here as a ground truth, performs accuracy in the order of magnitude better, still with the drawbacks of calibrated and redundant multi-camera systems for diminishing the occurrence of occlusions. Regarding the evaluation of the overall system design and implementation, experiments validated the usability and effectiveness of the system in an applied teleoperation setup. During the comparative teleoperation tests the median success rate was equal to 93.75% for the w and 94.17% for the w/o HF with no significant difference. The relatively low occurrence of errors (object dropped) indicates that the system was usable by different subjects with a relatively short training time (15 minutes); it is also an indication of the overall reliability of the tracking.

The NASA TLI questionnaire results (Figure 8) did not evidenced stress or discomfort of the participants, and questions on mental and physical effort reported answers close to the mid-range of the scale. Answers related to the perception of success in executing the task was high (median score 17 over 20), in agreement with the high success rate. Considering the teleoperation setup, it indicates the interface was intuitive to operate even after the relatively short training time.

Figure 9 reports the box plots of the average variability and the average grasping pressure during the fast and precise task in the two conditions. On one side, the presence of tactile feedback did not produce a significant direct reduction of the applied forces, both in the A and B tasks (see bottom plot) - medians for fast case: 37.45 mBar (w HF), 31.96 mBar (w/o HF); medians for precise case: 39.83 mBar (w HF), 51.64 mBar (w/o HF). Together with the relatively high success rate

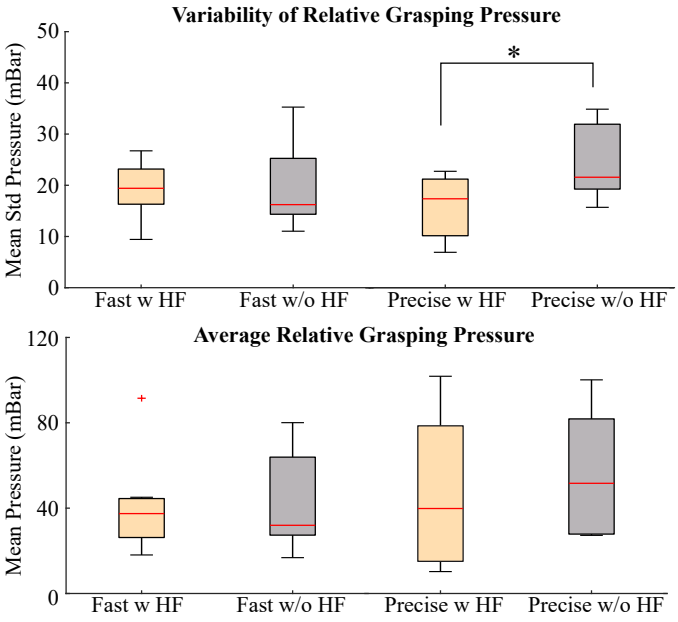

Fig. 9. Mean and mean standard grasping pressure across the telemanipulation tasks for different target objectives and tactile stimula (HF) - with (w) or without (w/o).

(object dropped) this can be explained by the dominance of the visual feedback, which allowed subjects to detect slippage even by direct sight, and by the fact that the rendered tactile feedback in the experiment was informative of grasping force modulation, but not of tangential slip. While the implemented actuators are capable of rendering high-frequency vibration and noise, hence informing to some extent of the occurrence of slippage, different sensors should be implemented on the robot side, in order to acquire such tiny signals. On the other side, the analysis of pressure variability over repetitions (see top plot) suggests that haptic feedback was indeed informative of grasping force modulation, guiding subjects to a modulation strategy more consistent between subsequent repetitions - medians for fast case: 19.41 mBar (w HF), 16.22 mBar (w/o HF); medians for precise case: 17.36 mBar (w HF), 21.57 mBar (w/o HF). The difference of variability in the precise test was statistically significant with a p-value of 0.0365.

V. Conclusions and Future Work

In this paper, we proposed a mechanical hand-tracking system based on adaptive linkage kinematics. With respect to other methods (i.e. vision tracking or data gloves), the purpose is to obtain robustness to occlusions and reliable finger tracking. This is relevant in certain applications such as teleoperation, where the uncertainty of tracking has direct effects in the physical world.

The design of the mechanism, and in particular the synthesis of the kinematics, was performed using the screw theory. The adopted methodology is presented, resulting in a multiple DoFs kinematic chain, parallel to the articular hand joints, and capable of adapting to different hand sizes with no singularities. Sensorization of the hand tracker joints allows for hand tracking at different finger segments. In the paper, we implemented and evaluated a prototype targeted for the teleoperation of the Prensilia MIA robotic hand, in terms of sensorized joints and controllable DoFs. The hand tracker structure enables the integration of compact haptic thimbles for the rendering of contact thresholds and fine modulation of the grasping force.

The hand-tracking system was validated in a complete teleoperation setup involving a fine pick-and-place task. The observed a low number of errors (objects dropped or not precisely placed in the housing) showed the effectiveness of the method even after short training periods. The role of tactile haptic feedback resulted less evident, probably due to the dominance of visual feedback and the absence of stick-slip rendering: nonetheless, it showed significant effects in reducing the variability of the grasping modulation across trials.

Future works include alternative haptic feedback solutions: we used here conventional voice coils capable of rendering the normal force, yet other cutaneous feedback cues (i.e. surface orientation or skin stretch) can be integrated with the proposed device and experimented in teleoperation. Further developments include also the extension of the tracking method to the full upper limb, in the shape of a light and wearable device, in order to obtain the full hand pose and position tracking with the same technology.

References

[1] T. Klamt, D. Rodriguez, L. Baccelliere, X. Chen, D. Chiaradia, T. Cichon, M. Gabardi, P. Guria, K. Holmquist, M. Kamedula, *et al.*, "Flexible disaster response of tomorrow: Final presentation and evaluation of the centauro system," *IEEE robotics & automation magazine*, vol. 26, no. 4, pp. 59–72, 2019.

[2] M. Schwarz, C. Lenz, A. Rochow, M. Schreiber, and S. Behnke, "Nimbro avatar: Interactive immersive telepresence with force-feedback telemanipulation," in *2021 IEEE/RSJ International Conference on Intelligent Robots and Systems (IROS)*. IEEE, 2021, pp. 5312–5319.

[3] F. Porcini, D. Chiaradia, S. Marcheschi, M. Solazzi, and A. Frisoli, "Evaluation of an exoskeleton-based bimanual teleoperation architecture with independently passivated slave devices," in *2020 IEEE International Conference on Robotics and Automation (ICRA)*, 2020, pp. 10 205–10 211.

[4] S. S. Rautaray and A. Agrawal, "Vision based hand gesture recognition for human computer interaction: a survey," *Artificial intelligence review*, vol. 43, no. 1, pp. 1–54, 2015.

[5] A. Tkach, A. Tagliasacchi, E. Remelli, M. Pauly, and A. Fitzgibbon, "Online generative model personalization for hand tracking," *ACM Transactions on Graphics (ToG)*, vol. 36, no. 6, pp. 1–11, 2017.

[6] G. D. Kessler, L. F. Hodges, and N. Walker, "Evaluation of the cyberglove as a whole-hand input device," *ACM Transactions on Computer-Human Interaction (TOCHI)*, vol. 2, no. 4, pp. 263–283, 1995.

[7] G. system, 2022/12, available on line. [Online]. Available: http://www.cyberglovesystems.com/

[8] C. Mizera, T. Delrieu, V. Weistroffer, C. Andriot, A. Decatoire, and J.-P. Gazeau, "Evaluation of hand-tracking systems in teleoperation and virtual dexterous manipulation," *IEEE Sensors Journal*, vol. 20, no. 3, pp. 1642–1655, 2019.

[9] M. Sarac, M. Solazzi, E. Sotgiu, M. Bergamasco, and A. Frisoli, "Design and kinematic optimization of a novel underactuated robotic hand exoskeleton," *Meccanica*, vol. 52, pp. 749–761, 2017.

[10] C. Pacchierotti, S. Sinclair, M. Solazzi, A. Frisoli, V. Hayward, and D. Prattichizzo, "Wearable haptic systems for the fingertip and the hand: taxonomy, review, and perspectives," *IEEE transactions on haptics*, vol. 10, no. 4, pp. 580–600, 2017.

[11] C. Coppola, G. Solak, and L. Jamone, "An affordable system for the teleoperation of dexterous robotic hands using leap motion hand tracking and vibrotactile feedback," in *2022 31st IEEE International Conference on Robot and Human Interactive Communication (RO-MAN)*. IEEE, 2022, pp. 920–926.

[12] L. Cappello, W. Alghilan, M. Gabardi, D. Leonardis, M. Barsotti, A. Frisoli, and C. Cipriani, "Continuous supplementary tactile feedback can be applied (and then removed) to enhance precision manipulation," *Journal of NeuroEngineering and Rehabilitation*, vol. 17, no. 1, pp. 1–13, 2020.

[13] D. Leonardis, M. Solazzi, I. Bortone, and A. Frisoli, "A 3-rsr haptic wearable device for rendering fingertip contact forces," *IEEE transactions on haptics*, vol. 10, no. 3, pp. 305–316, 2016.

[14] M. Maisto, C. Pacchierotti, F. Chinello, G. Salvietti, A. De Luca, and D. Prattichizzo, "Evaluation of wearable haptic systems for the fingers in augmented reality applications," *IEEE transactions on haptics*, vol. 10, no. 4, pp. 511–522, 2017.

[15] K. J. Kuchenbecker, J. Gewirtz, W. McMahan, D. Standish, P. Martin, J. Bohren, P. J. Mendoza, and D. I. Lee, "Verrotouch: High-frequency acceleration feedback for telerobotic surgery," in *International Conference on Human Haptic Sensing and Touch Enabled Computer Applications*. Springer, 2010, pp. 189–196.

[16] C. Pacchierotti, D. Prattichizzo, and K. J. Kuchenbecker, "Cutaneous feedback of fingertip deformation and vibration for palpation in robotic surgery," *IEEE Transactions on Biomedical Engineering*, vol. 63, no. 2, pp. 278–287, 2015.

[17] A. Di Guardo, M. Sarac, M. Gabardi, D. Leonardis, M. Solazzi, and A. Frisoli, "Sensitivity analysis and identification of human parameters for an adaptive, underactuated hand exoskeleton," in *Advances in Robot Kinematics 2018 16*. Springer, 2019, pp. 449–457.

[18] H. Li, L. Cheng, N. Sun, and R. Cao, "Design and control of an underactuated finger exoskeleton for assisting activities of daily living," *IEEE/ASME Transactions on Mechatronics*, vol. 27, no. 5, pp. 2699–2709, 2021.

[19] J. Lin, Y. Wu, and T. S. Huang, "Modeling the constraints of human hand motion," in *Proceedings workshop on human motion*. IEEE, 2000, pp. 121–126.

[20] I. M. Bullock, J. Borràs, and A. M. Dollar, "Assessing assumptions in kinematic hand models: a review," in *2012 4th IEEE RAS & EMBS International Conference on Biomedical Robotics and Biomechatronics (BioRob)*. IEEE, 2012, pp. 139–146.

[21] K. H. Hunt, "Structural kinematics of in-parallel-actuated robot-arms," 1983.

[22] X. Kong and C. Gosselin, *Virtual-Chain Approach for the Type Synthesis of Parallel Mechanisms*. Springer, 2007.

[23] Z. Huang, J. Liu, and D. Zeng, "A general methodology for mobility analysis of mechanisms based on constraint screw theory," *Science in China Series E: Technological Sciences*, vol. 52, no. 5, pp. 1337–1347, 2009.

[24] F. P. Schulter-Ellis and G. T. Lazar, "Internal morphology of human phalanges." *The Journal of hand surgery*, vol. 9.4, pp. 490–495, 1984.

[25] D. Leonardis, M. Gabardi, M. Barsotti, and A. Frisoli, "Discrete cutaneous feedback for reducing dimensions of wearable haptic devices." *Frontiers Virtual Real.*, vol. 3, p. 820266, 2022.